Journal of Colloid and Interface Science 337 (2009) 396–407

Contents lists available at ScienceDirect

Journal of Colloid and Interface Science

www.elsevier.com/locate/jcis

The impact of nanoscale chemical features on micron-scale adhesion: Crossover from heterogeneity-dominated to mean-field behavior

Ranojoy Duffadar [a], Surachate Kalasin [b], Jeffrey M. Davis [a], Maria M. Santore [c,*]

[a] Department of Chemical Engineering, University of Massachusetts, Amherst, MA 01003, USA
[b] Department of Physics, University of Massachusetts, Amherst, MA 01003, USA
[c] Department of Polymer Science and Engineering, University of Massachusetts, Amherst, MA 01003, USA

ARTICLE INFO

Article history:
Received 23 December 2008
Accepted 20 May 2009
Available online 23 May 2009

Keywords:
Interparticle force
Flocculation
Aggregation kinetics
Heterogeneity
Patchy surfaces
Heteroflocculation
Bacterial adhesion

ABSTRACT

This work explores the impact of nanoscale surface heterogeneity, small relative to the effective contact area between two surfaces, on pairwise colloid-scale interactions. Polycation-based positive patches, of order 10 nm in diameter, arranged randomly and lying flat on otherwise negative substrates, were used to create surfaces whose competing attractive and repulsive features determined the net interactions with opposing surfaces. Lab experiments and simulations of the adhesion of gently flowing dilute negative microparticles varied particle size (0.5–2 μm), ionic strength (κ^{-1} = 1–12 nm) and the density of heterogeneity on the collectors. Limiting behaviors from heterogeneity-controlled at high ionic strength to mean-field-like interactions at low ionic strength are reported. When heterogeneities are important, pairwise interactions are more attractive than predicted by average surface properties (e.g. per DLVO), and an adhesion threshold, describing the minimum average density of cationic features needed for single particle capture (adhesion), depends strongly on Debye length. In the opposite limit, the threshold becomes insensitive to the Debye length, and the average surface character approximates the interactions. An analytical treatment, reduced to a simple scaling argument predicts a −1/2 power-law dependence of the adhesion threshold on Debye length and particle size. A slightly stronger particle size dependence in experiments and simulations results from hydrodynamic contributions along with slight scaling differences in electrostatic, van der Waals, and hydrodynamic forces. An analogy to biological ligands is made for the heterogeneity-dominated limit: it is discovered, for this particular system, that engagement of as few as 20–100 cationic patches dictates particle adhesion (with details depending on flow, particle size, and ionic strength), similar to reports for selectin-mediated rolling of white blood cells during the inflammatory pathway. Also discovered is a heterogeneity-dependent crossover in the effect of ionic strength on particle capture, where added salt promotes particle adhesion in most cases but stabilizes the particles when the heterogeneity becomes relatively dense.

1. Introduction

All naturally-occurring surfaces are heterogeneous, with great chemical and topographical diversity. Synthetic interfaces (emulsions, foams, suspensions of micron- and sub-micron organic, inorganic, and polymeric particles) are sometimes geometrically and chemically simpler; however, heterogeneity usually exists in all but the most model of systems. Heterogeneity is an especially important feature of biological cells: for instance the clustering of receptors in phospholipid rafts potentially increases binding avidity. Of the two types of heterogeneity, chemical variations or roughness, works targeting the impact of the latter on force, friction, and adhesion are too numerous to review. For chemically homogeneous surfaces, roughness usually shifts the distance of closest approach between two surfaces and convolutes the interaction potential between smooth surfaces [1,2]. Pure roughness may also enhance the adhesion of small particles through an increase in the contact area (for particles of appropriate size), or shielding from hydrodynamic forces [3].

Long before the advent of chemical force spectroscopy to quantify chemical heterogeneities in systems including minerals [4–7], polymers [8–10], and biological cells [11–14], chemical heterogeneity was known to influence and even dominate colloidal forces and adhesion. For instance impurities on mineral surfaces often dictate aggregation [15–18], while small chemical features on polymer surfaces control contact angle and wetting [19–21], produce membrane fouling [22,23], enhance engineering adhesion [8,24,25], and determine biomaterial effectiveness [26–30]. Intracellular surface heterogeneities even govern biological processes such as the initial phases of leukocyte adhesion [31,32].

* Corresponding author. Fax: +1 413 545 0082.
E-mail address: Santore@mail.pse.umass.edu (M.M. Santore).

0021-9797/$ - see front matter © 2009 Elsevier Inc. All rights reserved.
doi:10.1016/j.jcis.2009.05.046

Electrostatic heterogeneity is understood to enhance bacterial adhesion [33] if not control it altogether (for some strains) [34,35]; it has been implicated in otherwise unexplained flocculation in colloidal systems [36–38], it is associated with defects in colloidal assemblies and crystals [39], and it has been used to flocculate particles in papermaking and waste-water treatment: patch-wise flocculation is accomplished with low molecular weight polymers of high cationic charge density, added in small amounts to negatively charged dispersions [40–45]. When the chains adsorb to individual negative particles in small amounts, they locally overcompensate the underlying negative charge, creating cationic nanoscale "patches" which are attracted to bare regions on other particles, producing aggregation. (The mechanism differs from bridging which requires higher molecular weight chains to reach between two particles.) The point-wise interactions between antigen- and peptide-presenting biomaterials and living cells are in some ways similar in physical principle to this example.

It is frequently reported, based on quantitative studies, that interaction forces or adhesion are "not additive," as they are dominated by heterogeneities or "hot spots" rather than reflecting the average surface character [46,47]. Attractions are often observed to be stronger, by orders of magnitude, than one would estimate from classical DLVO treatments where an area-averaged surface charge or potential (for instance approximated by zeta potentials) is employed [2,48–52]. Connecting to the current work, we note that the "additive" or "classical" DLVO is a "mean-field" approach, where one electrostatic potential and one Hamaker constant describe the surface.

A comprehensive understanding of how small-scale heterogeneity impacts colloidal forces is still forthcoming, as systematic experimental variations in heterogeneity are difficult. Only a few experimental systems have been developed to controllably vary heterogeneity, most of them with the heterogeneity lengthscales that approach those of the interacting objects or particles, or which utilize surfaces that are not entirely flat (thereby including some topography) [46,47,53–57]: in one exception, half-micron-scale latex deposition was employed to characterize unsaturated adsorbed layers of cationic polyelectrolyte at limited conditions where 2–3 polymer chains captured each latex particle [58,59]. In another, simulations reveal how hydrodynamics alter particle capture and release on surfaces with small heterogeneities [60]. Better experimental headway has been made through the variation of ionic strength, with the heterogeneous surface itself a fixed entity: ionic strength alters the structure of colloidal layers deposited on heterogeneous substrates [61], allowing larger numbers of particles to be deposited on submicron adhesive elements [57]. Increases in ionic strength also increase the particle capture rate on some surfaces with fixed heterogeneity [49].

Modeling of heterogeneity showed that it can impact the ultimate structure of deposited colloidal layers; however, early models assumed that single heterogeneity "elements" were each capable of adhering micron-scale particles, by virtue of their size [49,62] or binding strength [63]. While this assumption can sometimes hold [53,64], is not always the case and becomes less realistic for smaller surface asperities. Renormalization of mean-field expressions by integrating over the distribution of heterogeneity captures some features of experiment, but requires assignment of ionic-strength-dependent heterogeneity parameters [49].

The current work systematically examines of the impact of random chemical heterogeneity on pairwise interactions and dynamic adhesion, as exemplified by the capture of individual flowing particles on heterogeneous planar surfaces. We define "heterogeneity" as variations in surface chemistry at lengthscales at least an order of magnitude smaller than the area of interaction between two surfaces, so that many "features" may engage as surfaces approach. This definition excludes topographically complex surfaces or those with regular patterns or larger features, for instance micron or near-submicron elements or chemical stripes on a planar surface that interact with a microparticle. Indeed, in the current work, the primary action of the heterogeneous features is to provide tiny regions of high attractive energy. In principle, the feature size need not be proportional to its adhesion energy, though this is frequently the case and it is an issue we are examining separately.

Electrostatic heterogeneity is considered in this paper, using a model system consisting of a negative surface randomly decorated with flat cationic patches that are about 10-nm in size. The subsequent adhesion rates of flowing micron-scale particles, in the limit of low particle coverages, are dictated exclusively by collector-particle interactions, avoiding multi-particle interactions. Also presented are simulations incorporating hydrodynamic and colloidal interactions that match the experimental parameters, along with analytical and scaling treatments.

Within the electrostatic paradigm of a repulsive surface containing small random attractive elements, the current paper examines the effects of particle size, ionic strength, and the degree of heterogeneity over a much broader range than prior work, and combines simulation and experiment to reveal aspects of adhesion that are difficult to access by experiment alone. Two limiting regimes are explored. At high ionic strength, particle adhesion is dominated by the heterogeneity of the collector: microparticles adhere onto surfaces even though the net interactions (for instance, anticipated by DLVO based on the average surface charge/potential) would be repulsive. The adhesion is characterized by a particle-sensitive threshold that sets a minimum average density of attractive elements needed to capture particles, with the threshold sensitive to ionic strength. Simulations further reveal the number of cationic patches engaged in particle capture. Since, in this limit, the nanoscale cationic patches act as individual adhesive elements, an analogy to bioadhesion is made: depending on particle size and ionic strength, $O(10)$–$O(100)$ patches are required to capture each microparticle; although the number of patches per unit area of effective particle-collector contact is essentially constant. In the opposite limit, at low ionic strengths mean-field-like behavior is observed and the adhesion rate becomes insensitive to ionic strength.

The study reports an additional interesting observation, as the ionic strength is increased, crossing over from heterogeneity-dominated behavior to mean-field-like action: for surfaces with low densities of heterogeneity, ionic strength increases the rate of particle adhesion, analogous to flocculation, as is frequently found in the literature. Conversely, for surfaces that are slightly more attractive, due to a greater density of cationic patches, ionic strength detracts from the particle capture rate. This effective particle stabilization at increased ionic strength is seen both experimentally and in simulations and is a consequence of the randomness of the distribution of attractive heterogeneities, as added salt also screens the locally attractive regions of the surface.

In this paper, analytical and scaling arguments are also presented for the effect of ionic strength and particle size on the critical surface density of patches required for particle capture. The scaling exponent of $-1/2$ reflects the random distribution of adhesive elements and the effective contact area in a system whose interactions are predominantly electrostatic.

2. Description of the system

These studies utilize a system, shown in Fig. 1, in which microparticles of radius a and relatively uniform negative surface charge are gently flowed in simple shear over electrostatically heterogeneous collecting surfaces and their adhesion monitored. The heterogeneous nanofeatures on the collector are electrostatically attractive while the main portion of the collecting surface is electrostatically repulsive towards approaching particles.

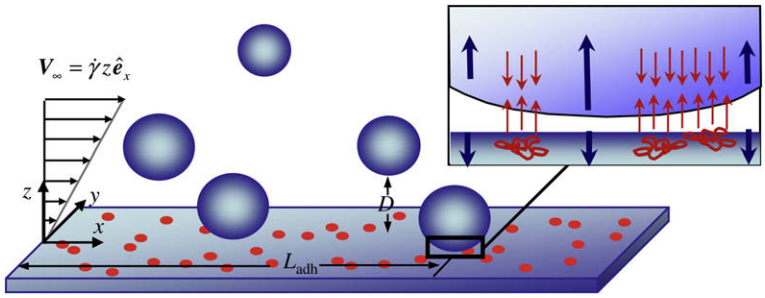

Fig. 1. Schematic of system, illustrating how 11-nm adsorbed cationic polymer coils act as randomly-distributed adhesive patches that can capture particles from a flowing, monodisperse suspension.

For simplicity, the surface potentials of the negative and positive regions of the collecting surfaces are equal but opposite in sign, and the negative portion of the collector is the same as the microparticles themselves. This is accomplished experimentally by adsorbing cationic polymer coils (poly(dimethylaminoethyl methcrylate)), pDMAEMA, with R_h = 4.5 nm and R_g slightly larger to give the 11 nm diameter [65], at sub-monolayer coverages onto a negatively charged silica flat [66,67]. We refer to the resulting isolated adsorbed polycation chains as "patches," in Fig. 1. The charge on these cationic patches is sufficiently dense that the adsorbed chains lie flat to the surface at the conditions of study, with nearly 100% trains [68]. The dense positive charge of the adsorbed polycations also locally overcompensates the underlying negative charge of the silica, similar to that known to occur in "patch flocculation" [40,41,43–45]. As the pDMAEMA is a weak polyelectrolyte, the buffer pH of 6.1 was chosen so that the polycation was strongly charged, and so that a saturated layer of pDMAEMA exhibited a positive electrophoretic mobility that was roughly equal (but opposite in sign) to that of bare silica at the same conditions (3.5 and -3.5×10^{-8} m^2/Vs, respectively corresponding roughly to −50 and +50 mV. This corresponds to 14–15 uncompensated positive charges per patch) [66,69]. We have also confirmed that the adsorbed patches are not displaced or transferred during these experiments, nor do they exhibit any lateral mobility [70].

It is also worth mentioning that at the saturation coverage of 0.45 mg/m^2 [69,71], the collecting surfaces bear relatively uniform positive charge. This condition represents nominal 100% coverage of the surface by the polycation. The surfaces are net negative below coverages of 50%, or 0.225 mg/m^2, corresponding to an average center–center patch spacing of ∼15 nm [66]. This work focuses on surfaces which are net negative, or which have average patch–patch spacings greater than about 20 nm. It is a coincidence, that for these 11 nm pDMAEMA coils, the % coverage (defined simply relative to a saturated surface) corresponds roughly to the occupied area of the surface, allowing a close comparison with simulation.

The simulations have been designed to match the experiments, leaving no adjustable parameters. Negatively charged surfaces of both the collector and the spherical particles were assigned surface potentials of −50 mV, while the positive patches on the collector were +50 mV. Round cationic patches, 11 nm in diameter, were placed randomly on the collector (yielding Poisson statistics), to generate each collecting surface having a nominal area fraction occupied by cationic patches [66]. Colloidal forces between the sphere and the collector were calculated by the grid surface integration (GSI) method [72], employing a non-retarded Hamaker constant of 5×10^{-21} J for both positive and negative surface regions. The electrostatic double layer interactions between the each particle and the heterogeneous collector were based on the constant surface potential approximation to the linearized Poisson–Boltzmann equation. The GSI method is based on the discretization of two interacting surfaces of arbitrary geometry and heterogeneity, with subsequent integration to yield the total interactions (force or potential) at each point in the simulation. It will become apparent in the results that, though this approach adds electrostatic and van der Waals forces in manner that may seem similar to DLVO, the integrative GSI approach produces fundamental and substantial differences relative to DLVO that are effective in explaining counterintuitive experimental results. The colloidal (electrostatic and van der Waals) forces are combined with hydrodynamic forces via a mobility-matrix formulation of the low Reynolds number flow problem to determine the translational and rotational velocities, and thus the trajectory of a particle near a heterogeneous surface. With the simulations predicting the tractories of single particles flowing over the patchy surfaces, over a thousand such trajectories were run on different surfaces to determine the particle capture kinetics corresponding to an individual experimental data point. The number of trajectories and size of the collecting surface were chosen sufficiently large that a further increase had a negligible influence on the computed deposition rates, thereby ensuring convergence of the results.

3. Experimental details

Poly(dimethylaminoethyl methacrylate), pDMAEMA, a gift from DuPont was 31,300 in molecular weight. It was transferred from its original THF solution to water and then phosphate buffer as previously described [69,73]. The substrates, acid-etched microscope slides (Fisher Scientific, Pittsburgh, PA) were soaked in concentrated sulfuric acid overnight to produce substrates with a 10-nm layer of silica on their outer surfaces [74]. Phosphate buffer solutions with pH 6.1 were made using 0.0234 M KH_2PO_4 and adding a small amount of NaOH to reach the final pH. This solution was diluted as necessary with DI water to produce the more dilute buffer solutions. We found negligible pH variations with dilution in this range. The more concentrated buffer solution for a 1 nm Debye length was based on a 0.0936 M KH_2PO_4 solution whose pH was adjusted slightly by the addition of dilute NaOH.

Monodisperse silica particles were purchased from a variety of sources. Data reproduced here from a previous paper using 460 nm particles employed a modified in-house Stober synthesis [75,76] in which a rhodamine-tagged core was surrounded by several layers of non-fluorescent regular silica, as described in the original paper [66]. New data with 1 μm particles employed a sample from Gel-Tech (Orlando, Fl). Two-micron particles were purchased from Bangs Labs (Fisher, IN).

Heterogeneous surfaces were created by flowing a 20 ppm pDMAEMA solution in 0.026 M buffer over a microscope slide in our laminar slit flow cell (at a wall shear of 5 s^{-1}) for a controlled period of time, and then switching back to the same buffer. At this ionic strength for deposition, the Debye length is sufficiently small so that the chains are random coils. Based on a lack of mobility at

the conditions of study, we expect that variations in ionic strength during particle capture did not facilitate rearrangements of the adsorbed polymer coils [70,77]. Also, at these deposition conditions, the transport-limited deposition rate has been well-studied by optical reflectometry, so precise timing during the adsorption produces tight (±0.005 mg/m^2) control over the density of polymer deposited [65,66]. After 5 additional minutes of buffer flow at these conditions, the flow chamber was switched to a second buffer appropriate to the conditions for a particular particle deposition study. It is worth noting that though particle deposition was studied for a broad range of ionic strengths, the conditions for collector fabrication (ie. polymer adsorption) were constant. We checked that polymer was retained when the buffer was switched to that for the particle adhesion studies.

After 5 min of flow of the second buffer, a 0.1 wt% particle suspension in the second buffer was flowed over the test surface and particle deposition monitored either by optical reflectometry or directly in a lateral microscope. In both methods, the flow chamber was oriented with the test surface perpendicular to gravity so that only colloidal and hydrodynamic forces influenced particle capture. The particle deposition rate was linear in particle flow time for many tens of minutes, providing a large window over which to measure the particle deposition rate before surface crowding reduced the particle capture rate. The particle adhesion in this linear regime was interpreted to reflect pairwise particle-collector interactions.

For studies employing optical microscopy to track particle deposition, video footage was analyzed frame-by-frame to determine particle capture rates using Image-J software. In the case of optical reflectometry, the signal at short times is linear in the particle surface coverage, and transport-limited particle capture on highly adhesive cationic surfaces was employed to establish a calibration constant, as previously described [66].

4. Simulation detail: from single particle trajectories to deposition rates

Duffadar and Davis have developed a simulation scheme, the Grid Surface Integration (GSI) method, to compute colloidal interactions (electrostatic double layer, van der Waals) between particles and surfaces, either (or both) of which can have arbitrary shape and chemical heterogeneity. They have combined this method with a mobility-matrix formulation of particle hydrodynamics to predict trajectories of single particles in shear flow over heterogeneous surfaces. As detailed descriptions of the simulations are lengthy and have been published previously [72,78], we will not repeat them here. At the level of individual particles, the method predicts particle adhesion (as evidenced by very close approach, or contact between nanometer-scale roughness elements on the surfaces) on surfaces whose patch densities fall above the adhesion threshold, and no particle adhesion on surfaces whose patches densities fall below the threshold. Quantitative comparison with experiment, in the current work, however, requires the translation of single particle trajectories to macroscopic particle accumulation rates.

The probabilistic approach, developed here for the prediction of particle deposition rates from a flowing suspension, employs roughly $T_{total}(\rho) = 1000$ simulations of single particle trajectories over different surfaces carrying the same overall patch density, ρ, but varying in the details of the random patch arrangements. Prediction of a deposition rate datum (corresponding to a single experimental run) involves determination of the average effective surface length (travel distance) and average travel time before a single particle adheres to the collector for the ~1000 simulations. Because the colloidal interactions come into play only for relatively small particle separations, it is assumed that particle transport from the bulk solution to the region near the heterogeneous collecting surface occurs at the transport-limited rate, which is calculated from the Leveque equation for diffusers in a slit shear cell [79]. (Additional simulations performed with Brownian forces included explicitly via a Gaussian-distributed stochastic noise term yielded identical results for the deposition rates for the parameters used in this study.) Once a particle is sufficiently close to the surface, the local surface landscape, comprising van der Waals and patchy electrostatic interactions, determines the particle trajectory and adhesive (or not) fate. Of the total number of trajectories, $T_{total}(\rho)$, for a given surface patch density, flow rate, particle size, and ionic strength, some number, $T_{arrest}(\rho)$, lead to particle contact and adhesion. For this study, the capture criterion is that the separation distance between the particle and surface drops below 1 nm. Additional simulations with different cutoff values exhibited negligible differences in the computed deposition rate curves provided the critical separation distance for adhesion was taken to be less than approximately 2 nm. (Analogous results are obtained using the more detailed model of Duffadar and Davis [78] that accounts for particle rolling if a sufficiently large and experimentally relevant value of the coefficient of rolling friction is employed.) If particle adhesion occurs, L_{adh} represents the translational distance covered by the particle before it adheres, and t_{adh} denotes the elapsed time before particle adhesion, each for the particular particle of study.

Libraries of heterogeneous surfaces, with thousands of different random surfaces for each single patch loading, ρ, were needed for this work. To create these, each surface was initially discretized into a square grid, the optimal size of which was previously discussed [72]. The appropriate numbers of these grid elements, for a particular average patch loading, were assigned a randomly-located positive patch, using a Gaussian random number generator in Intel FORTRAN to yield Poisson statistics. The remaining patches were negatively charged. This method ensures that the placement of each patch is independent of the location of other patches, though the patches may not overlap. The approach is consistent with the screening of the inter-coil repulsion during pDMAEMA deposition at the substantial ionic strength used in the experiments.

For each datum, corresponding to $T_{total}(\rho)$ simulated trajectories (order 1000), the probability of particle adhesion is given by:

$$P_{adh}(\rho) = \frac{T_{arrest}(\rho)}{T_{tot}(\rho)} \tag{1}$$

The mean distance traveled, $L_{mean}(\rho)$ and mean time taken $t_{mean}(\rho)$, prior to particle adhesion are defined:

$$L_{mean}(\rho) = \frac{\sum_{k=1}^{T_{tot}(\rho)} \xi_k L_{adh,k}}{T_{arrest}(\rho)} \quad t_{mean}(\rho) = \frac{\sum_{k=1}^{T_{tot}(\rho)} \xi_k t_{adh,k}}{T_{arrest}(\rho)} \tag{2a, b}$$

Here for the kth simulation, $\xi_k = 1$ if the particle ultimately adheres, and 0 if it does not. The probability of particle adhesion $P_{adh}(\rho)$ is then combined with L_{mean} to obtain an average effective surface length $L_{adh,eff}(\rho)$ required to adhere a single particle on a surface of average patch loading, ρ. Similarly, an effective time, $t_{adh,eff}(\rho)$, required for particle adhesion is found by combining $P_{dep}(\rho)$ with $t_{mean}(\rho)$.

$$L_{adh,eff}(\rho) = \sum_{k=0}^{\infty} \{1 - P_{adh}(\rho)\}^k P_{adh}(\rho) L_{mean}(\rho) + kL_{total}\} \tag{3a}$$

$$t_{adh,eff}(\rho) = \sum_{k=0}^{\infty} \{1 - P_{adh}(\rho)\}^k P_{adh}(\rho) L_{mean}(\rho) + kt_{total}\} \tag{3b}$$

Here, L_{total} is the extent of the surface used for the simulations and is typically 20–30 times the particle diameter, while t_{total} is the time

required for the particle to flow over this length of surface without contact. The approach of summing an infinite series in Eq. (3) is analogous to modeling a much larger domain using periodic boundary conditions, and removes the dependence of the results on the (finite) length of the surface used in the simulations. This makes it particularly advantageous for simulations on surfaces with ρ near the adhesion threshold, for which the adhesion rate is small. A simulated particle deposition rate, $d\Gamma_{sim}/dt$ can be computed as

$$\frac{d\Gamma_{sim}}{dt} = \frac{4\pi\rho_{SiO_2}a^3}{3}\frac{1}{L_{adh,eff}(\rho)Wt_{adh,eff}(\rho)}. \quad (4)$$

Here, ρ_{SiO_2} is the density of silica, and W is the width of the heterogeneous surface, taken as $2a$. This simulated particle deposition rate is then renormalized relative to the maximum, transport-limited rate, to take into account flow cell geometry, and transport effects involving the arrival of the particle at the near-surface regime which comprises the staring point for each simulated trajectory:

$$\frac{d\Gamma}{dt}(\rho) = \left.\frac{d\Gamma}{dt}\right|_{transport\ \ limited}\left(\frac{\frac{d\Gamma_{sim}}{dt}}{\frac{d\Gamma_{sim,max}}{dt}}\right) \quad (5)$$

Here $d\Gamma_{sim,max}/dt$ is the maximum value of the simulated deposition rate for each set of experimental conditions (patch density, particle size, flow rate, ionic strength, etc.). This renormalization obviates the need for the multiplicative factor of $4\pi\rho_{SiO_2}a^3/3W$ in Eq. (4), which is included only to yield the proper units in the intermediate results for $d\Gamma_{sim}/dt$. The expression developed in Eq. (5) is appropriate for comparison to experimental measurements using dilute suspensions in a flow chamber.

A few general comments about this simulation approach are worth noting: First the study of single particle behavior on heterogeneous surfaces, employing a library of thousands of randomly generated surfaces turns out to be an effective tool for comparison to experimental systems that involve many particles but are still dominated by pairwise particle–surface interactions. The experimental conditions in this paper correspond to the dilute particle limit, making the single particle simulation runs appropriate. Second, while Brownian effects are important in controlling the diffusion of particles from the bulk to the near-surface region, they turn out not to influence the particle behavior near the surface itself. We established this in simulations [80] which included multiple effects for the stochastic term [81–83]. These more involved simulations gave the same overall behavior as presented here for a variety of surfaces with different overall patch densities [80]. Finally, while starting the particle trajectory simulations at the secondary minimum appears arbitrary, the normalization procedure described here facilitates a translation from many single-trajectory runs to macroscopic deposition rates that are independent of the initial condition of the trajectory simulations.

5. Results

5.1. Particle size and ionic strength: a range of behaviors

Compared in Fig. 2 are the simulated and experimentally observed particle capture rates (lines and symbols, respectively) on a series of surfaces, with varying cationic patch content on the x-axis. The x-axis units are % positive patches, based on a saturated

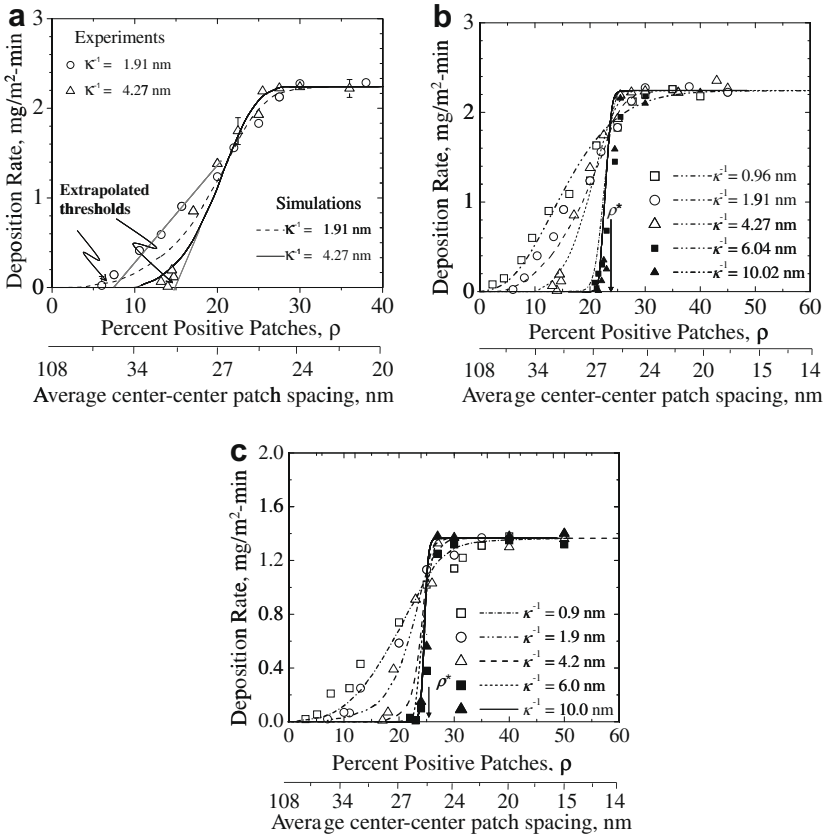

Fig. 2. (a) Simulated and experimentally observed rates of 1 μm silica particle capture on patchy surfaces, for two ionic strengths. Also shown are two adhesion thresholds, for the experimental data at $\kappa^{-1} = 1.91$ nm and the calculations at $\kappa^{-1} = 4.24$ nm. (b) Simulated and experimentally observed capture rates of 1 μm particles on surfaces of different patch densities. Each ionic strength is a single data set. The density of patches at the crossing point, ρ^*, is indicated. (c) Simulated and experimentally observed capture rates of 2 μm particles on surfaces of different patch densities. Each ionic strength is a single data set.

pDMAEMA layer of 0.45 mg/m^2 for 100%. For this particular system, 50% patches corresponds to a nearly net neutral collecting surface. Further, for this system, it is coincidental that the fractional mass coverage corresponds to the fractional area coverage of the simulations, ρ. Part a of Fig. 2, for 1 μm particles, focuses on ionic strengths of 0.026 and 0.005 M, corresponding to Debye lengths of 1.96 and 4.24 nm. The experiments in part a are similar to those previously published [66,67], but are more precise as a result of the use of the lateral microscope rather than near Brewster reflectometry. The newly simulated particle capture rates are in excellent agreement with the experimental observations, as there are no adjustable parameters, indicating that the experimental system is sufficiently well characterized and understood.

Important features of the individual data sets (at fixed ionic strength) in Fig. 2a include: (1) a lack of particle capture on surfaces with extremely low levels of cationic features; (2) a threshold denoting the minimum average density of cationic patches needed for particle capture; (3) a regime, at greater cationic patch surface densities than the threshold, in which the particle capture rates are sensitive to the collector composition; and (4) a regime, here above about 25% cationic patch density, in which the collector is net negative but particles adhere at the transport-limited rate. (This limiting rate is determined quantitatively, for a particular particle size and flow rate in our chamber, and confirmed experimentally [66]). Additionally, comparing data sets or "rate traces", reveals two effects of Debye length: the threshold shifts to greater patch densities with larger κ^{-1} and, in addition, the rate traces become steeper. These effects give an interesting crossing of the two data sets.

We wish to emphasize that for collectors containing fewer than 50% patches, the surface is net negative. Substantial particle adhesion is observed with patch densities slightly greater than the adhesion thresholds, corresponding to very negative surfaces. Hence Fig. 2 documents strong overall colloidal attractions onto surfaces which are net negative, a behavior which contradicts predictions of DLVO theory, even when van der Waals forces are included in the calculation. The favoring of localized attractions over the repulsive interactions (which cover a larger substrate area) is a result of the random heterogeneities.

The significance of an adhesion threshold is worth noting: a threshold, or a finite x-intercept, indicates that multiple cationic patches are needed to trap a silica particle. By contrast, were the particle capture rate, as a function of patch density, to pass through the origin, then any collecting surface would, as long as it contained at least one cationic patch, be able to capture a microsphere, albeit very slowly [64,66,67].

Considered in part b of Fig. 2 is a broader range of ionic strengths, still for 1 μm particles, now corresponding to Debye lengths from 1 to 10 nm. At high salt concentrations or small Debye lengths, the threshold is small and the particle capture rate grows relatively gradually as the density of adhesive cationic patches is increased, on the x-axis. In this limit, the surface is far more adhesive than one would estimate by its average surface charge, even including van der Waals interactions. This result corroborates various observations/speculations in the literature that heterogeneity enhances the attractive component of the interaction [33,35–37,48,49]. In the limit of large Debye lengths, both experiment and simulated rate traces converge to a steep shape, independent of the Debye length. Here, if microparticle adhesion occurs at all, it is transport-limited.

Presented in Fig. 2c are experimental and simulated data for 2 μm particles and the same range of ionic strengths. Here the same trends are qualitatively observed, with excellent agreement between simulations and experiments. The slight differences between the 1 and 2 μm particles include greater values of the adhesion threshold for the larger particles at the same ionic strength, and a slower transport-limited particle capture rate. The latter is expected since large particles diffuse more slowly than small ones.

Recapitulated in Fig. 3 are the data of Fig. 2b explicitly as a function of ionic strength on the x-axis, to facilitate comparison with the literature [49,84,85]. Data for several different densities of cationic patches, with each patch density on a different curve, highlight the striking result that added salt can help or hinder particle capture. On surfaces with low patch densities, increases in ionic strength cause an increased particle capture rate. Increased particle adhesion or flocculation with added salt has been long reported in the literature, albeit with surfaces whose heterogeneities were not characterized and homogeneity was implied by use of DLVO-related arguments. We find one report of calculated increased flocculation with added salt in a heterogeneous system [49]. With the greatest patch densities on the collector in Fig. 3 (30% and 40%), particle capture is insensitive to ionic strength due to bulk solution transport limitations on particle capture. However, for collectors whose patch densities are large, but fall short of the transport-limited regime, (for instance 27% patches), the particle adhesion rate is unexpectedly reduced with increasing ionic strength.

DLVO theory predicts that, with the addition of monovalent electrolyte, the net interactions between like-charged homogeneous surfaces become more attractive due to electrostatic screening and the increasing relative importance of van der Waals attractions. Thus addition of salt to electrostatically-stabilized suspensions of homogeneous particles increases the aggregation rate. One concludes that a similar effect occurs for our system when surfaces have less than 25% patches: here the primary effect of added monovalent electrolyte may to be screen the electrostatic repulsion, allowing both van der Waals attractions and the electrostatic attractions from the patches to increase the particle capture rate. For surfaces with greater densities of cationic patches, however, still falling short of transport-limited particle capture, the effect of salt is to weaken both the attractions and repulsions. Apparently, in Fig. 3, in this regime with electrostatic attractions being relatively important, added salt actually has a stabilizing effect, due to the interaction of spatial fluctuations in the local patch density, the size of the electrostatic zone of influence, and the strength of the (screened) electrostatic interactions.

Summarized in Fig. 4 is the dependence of the adhesion thresholds from Fig. 2 on particle size and ionic strength. The symbols represent experimental data while the curves are the simulation

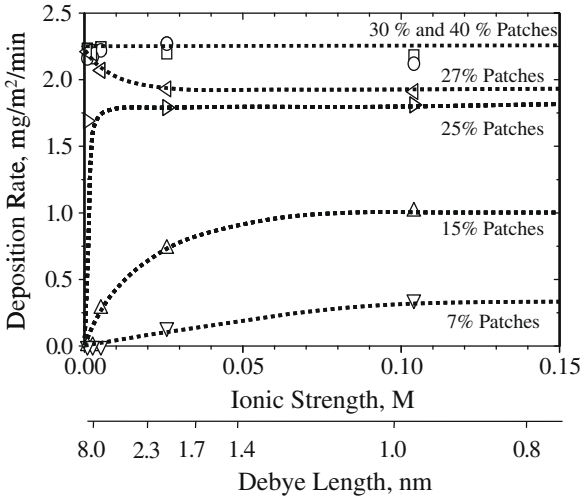

Fig. 3. Experimental data from Fig. 2b for 1 μm particles, recast with ionic strength as the independent variable. Curves here simply guide the eye.

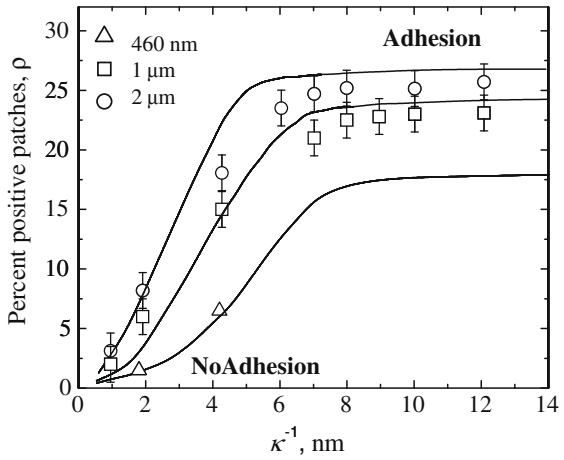

Fig. 4. Loci of adhesion thresholds as a function of the Debye length, for three particle sizes. The 460 nm were taken from Ref. [63].

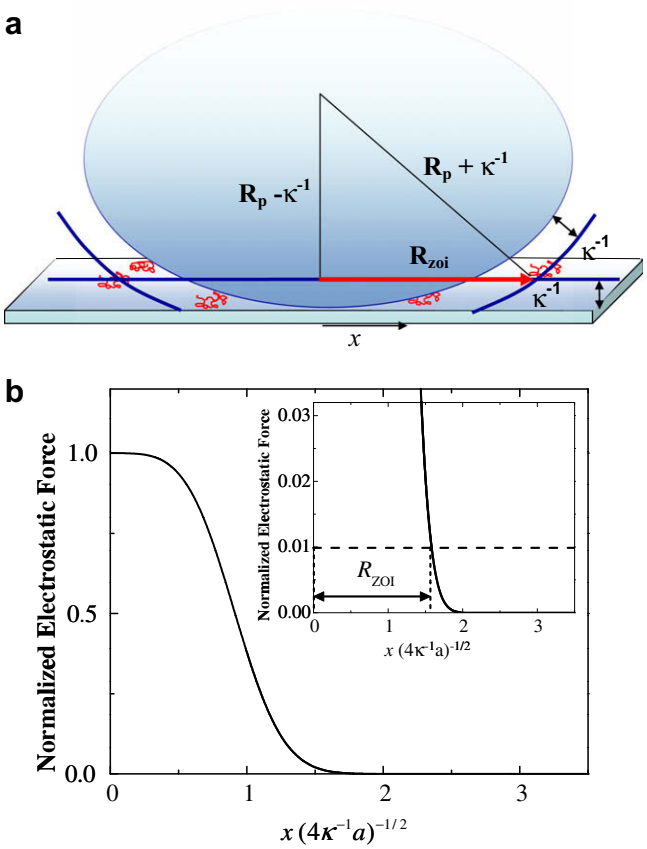

Fig. 5. (a) Geometric definition of the zone of influence having radius, R_{zi}. (b) The electrostatic force as a function of radial position, x (defined in Fig 5a), for a sphere interacting with a plate. Calculations here are for two Debye lengths, 4.24 and 13.8 nm. These collapse to a single curve when the x-axis is scaled as shown.

results. There is, again, strong agreement between experiment and theory. Included in Fig. 4 are data for 460 nm particles from a previous paper [66], and new simulations for these smaller particles as well. Two limiting behaviors are observed. First, for small Debye lengths, the adhesion threshold extrapolates to zero. This suggests that only for the smallest Debye lengths are individual patches able to capture flowing silica particles. This behavior contrasts with prior reports of particle capture by immobilized attractive nanoparticles which protruded forward of the surface and could each capture silica microspheres at finite Debye lengths [53]. In Fig. 4 for large Debye lengths, the Debye length has only a slight effect on the threshold for particle capture, though the threshold is still sensitive to particle size. Thus, two limiting behaviors are borne out in Fig. 4: the fluctuation-dominated limit at small Debye lengths and a mean-field-like limit at large Debye lengths.

5.2. The key role of contact area

An understanding of these limiting behaviors follows from the identification of key lengthscales. Because the different forces (electrostatic, van der Waals, hydrodynamic) scale differently with particle size and other parameters, a particular form to collapse the data in Figs. 2–4 is not obvious. The radius of the effective contact area between the spheres and the collector is an important lengthscale that depends on particle size and ionic strength, as illustrated in Fig. 5a. Here a Debye shell around the particle intersects (a Debye cushion over) the planar surface. Hence the area on the planar surface is termed the (electrostatic) zone of influence, and its radius R_{zoi} follows from geometry: $R_{zoi} = 2(\kappa^{-1}a)^{1/2}$.

If one considers a sphere near a plate, the electrostatic force decreases radially in the plane of the flat surface, from the point of closest approach, as shown in Fig. 5b. A second definition of the zone of influence, apparent in the simulations and entirely consistent with that in Fig. 5a, is that R_{zoi} is the approximate radial distance from the contact point where the electrostatic force has dropped to 99% of its value at contact or closest approach. In Fig. 5b, this electrostatic force is calculated for 2 Debye lengths, and the scaling from the geometric argument in Fig. 5a collapses them exactly.

Particle adhesion requires that a sufficient number of adhesive patches be present in the zone of influence as a particle approaches the surface. Because the local patch density fluctuates spatially (due to the random statistical nature of the patch deposition process), some regions of the surface are more adhesive than others. When the zone of influence is small (at high ionic strengths or with sharply curved particles), it can be relatively easy for a particle to find a (locally attractive) surface region containing a substantially above-average number of patches. Here the particle will tend to adhere. Conversely, when the zone of influence is large (for large particles or low ionic strengths), an approaching particle samples a more nearly average surface character. Since the surface is net negative this tends to be repulsive. A larger average number of patches is therefore required for particle capture, which results in a shift of the threshold to higher patch densities at low ionic strengths or for large particles.

When the Debye length exceeds about 8 nm for the 1 μm particles (or 6 nm for the 2 μm particles), the thresholds in Fig. 4 and indeed the shapes of the rate plot in Fig. 2 become less sensitive ionic strength. At this point the zone of influence has become relatively large, so that particle capture is mostly sensitive to the average surface character. We therefore term this regime of behavior as being mean-field-like. It is important to note that the Debye lengths corresponding to the onset of this mean-field-like behavior, (6–8 nm) are still smaller than the average patch spacing near the threshold, which is always greater than about 25 nm. Thus throughout this work the cationic patches are fundamentally isolated from each other by negative surface charge. In the mean-field-like limit, particle capture remains sensitive to particle size due to the particle size sensitivity of Van der Waals and integrated electrostatic forces, for instance as described by DLVO theory. Hydrodynamics, with their particle size-squared dependence of shearing forces [86], also contribute to the influence of particle size, favoring the adhesion of small particles over larger ones.

5.3. Domination by heterogeneities

As the observation of an adhesion threshold signals that multiple adhesive features are required for particle capture, it is obvious to ask how many adhesive patches are actually involved. We are not able to access this information experimentally; however, the excellent agreement between simulated and experimentally observed particle capture rates in Fig. 2 suggests that simulated results for the number of patches involved in particle capture are relevant.

The numbers of patches involved in particle capture was determined by examining the surface features beneath adherent particles in the many simulation runs making up Fig. 2. Approximately 1000 simulations were conducted for each density of cationic patches on the substrate and for each ionic strength and particle size. Once a particle had arrested on the surface, the number of patches beneath it, within the zone of influence (the circle of radius R_{zoi} centered under the particle), was determined. Illustrated in Fig. 6a are the numbers of cationic patches found in the zone of influence for simulations covering a subset of the conditions in Fig. 2b: 1 μm particles adhering at Debye lengths from 1–8 nm. Each datum in Fig. 6a represents the average of at least 1000 simulation runs, with typical statistics shown in Fig. 6b, for three arbitrary data points.

In Fig. 6a, at fixed Debye length, the average number of patches in the zone of influence (y-axis) beneath adherent particles increases only slightly as the average patch loading on the surface (x-axis) is increased. This slight increase suggests that particles adhere at the first opportunity rather than diffusing gradually on the surface to the most adhesive region. That is, even though the average patch concentration is increasing on the x-axis of Fig. 6a, there are still regions of surface with small numbers of patches, still above the critical capture concentration. The particles adhere to these spots rather than continuing a search for a more favorable place to settle.

The most dramatic feature of Fig. 6a is how the ionic strength affects the patch density needed for particle capture, as shown on the y-axis. This dependence on ionic strength is a consequence of the increasing size of the zone of influence with ionic strength ($R_{zoi} \propto \kappa^{-1/2}$). This point is further emphasized in Fig. 6c, which contains plots of the minimum numbers of patches at the thresholds in the zone of influence needed for particle capture for different ionic strengths and particle sizes. (The 460 nm diameter particles were simulated for comparison with data in a prior publication [66].) The requirement for greater numbers of patches to capture larger particles is expected because the size of the zone of influence and the hydrodynamic forces increase with particle size.

An interesting aside is borne out in Fig. 6c: one can compare the average numbers of patches involved in particle capture in these gentle shearing conditions (39 s^{-1}) to the numbers of ligands and receptors engaging to facilitate the capture biological cells from flowing streams. The ball-park numbers in our simple system can be quite small, considerably less than 50 at physiological ionic strengths corresponding to κ^{-1} of 1 nm or less. Extrapolating the trends in Fig. 6c up to 8 μm spheres, the size of leukocytes, one still finds small numbers of patches involved in particle capture, on the order of 50. Our observations with this non-biological system therefore are strikingly close to the estimations of 20–100 selectin bonds engaged to sustain leukocyte rolling on injury-activated endothelium [87,88].

The data of Fig. 6c are condensed in Fig. 6d to show how the minimum number of patches needed for particle capture (corresponding to the adhesion threshold) varies with particle size and ionic strength, with the patch number normalized by the area of the zone of influence to give a local surface concentration. It should be emphasized that the surface concentrations in Fig. 6d result from the spatial fluctuation of patches and represent "hot spots" that are sticky enough for particle capture rather than the average surface concentration. The remarkable observation in Fig. 6d is that the local patch concentration that enables particle capture is virtu-

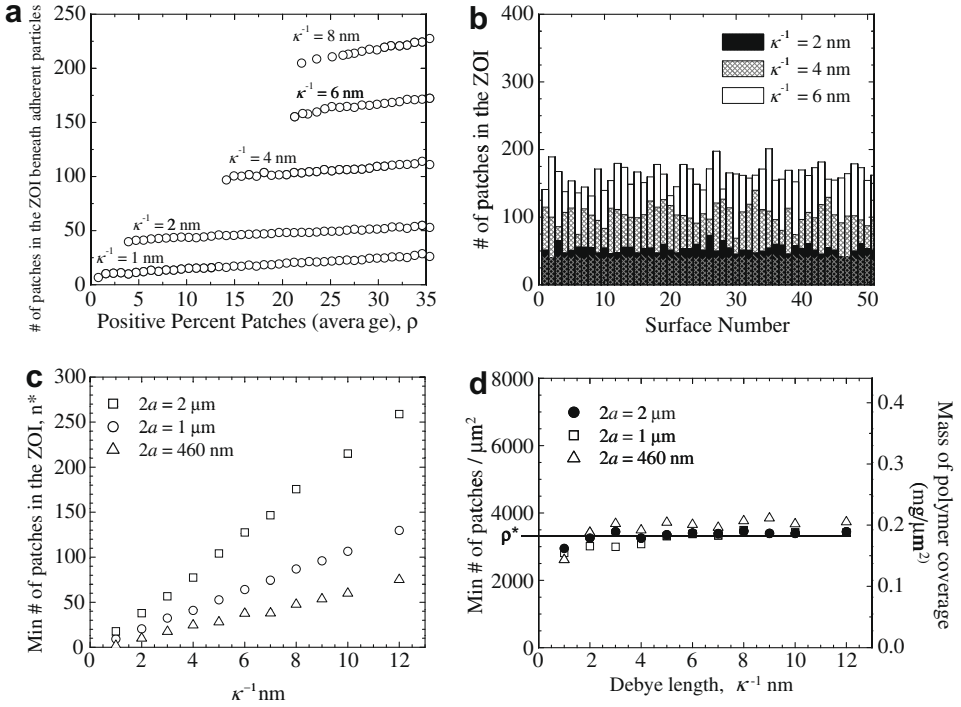

Fig. 6. (a) The average number of patches in the zone of influence beneath adherent 1 μm particles as a function of the percent positive patches originally loaded onto the surface. This x-axis is the same as those in Fig. 2. (b) Example statistics for 50 surfaces at each ionic strength in (a), for surfaces having a 23 percent positive patches. (c) The number of patches needed, at the adhesion threshold, to capture a microparticle for surfaces containing slightly greater than the threshold loading of positive patches. (d). Renormalization of data in (c) on the size of the zone of influence. Similar data for 460 nm and 2 μm diameter particles are also included.

ally independent of ionic strength, save a slight 10% increase as the ionic strength is varied over the full experimentally practical range. The impact of particle size on the critical local concentration is equally small. This insensitivity to particle size, in particular, suggests that colloidal interactions (electrostatic and, potentially, van der Waals) far outweigh hydrodynamic interactions, even though the latter scale as the particle size squared. This dominance by the colloidal forces is expected for the gentle shear conditions of the current study. Shear effects become more conspicuous as one considers a broader range of flow rates, as the threshold was found to scale with wall shear to the 1/3 power [89].

For the particular system of silica with pDMAEMA cationic patches at pH 6.1, it is observed that slightly more than 3000 patches/μm^2 of collector are needed for particle capture, corresponding to 0.157 mg/m^2 (or about 33% of saturation) locally in the zone of influence. This concentration is much greater than the average concentration at the adhesion threshold, which varies from 2% to 22% or 0.009–0.099 mg/m^2 as the Debye length is increased from 1–8 nm for a 1 μm particle. The random nature of the surface, which makes such fluctuations possible, is therefore key to particle capture at these conditions than would otherwise be non-adhesive.

Further, it is worth emphasizing that the local patch concentration for particle capture must depend on the nature of the underlying substrate. While the silica–silica repulsion at pH 6.1 is substantial, this background repulsion increases with pH as a result of the silica charge density. One would expect, therefore, even greater concentrations of cationic patches needed for particle capture at higher pHs.

5.4. From statistical to mean-field interactions

The observation of a nearly fixed local concentration of cationic patches forming an adhesive criterion for particle capture motivates an exploration of the statistical nature of particle capture and the crossover from fluctuation-controlled capture to mean-field-like behavior. Though a purely statistical approach neglects hydrodynamic effects and the impact of particle trajectory upstream of the capture location, we performed the exercise of calculating the probability for particle capture, assuming a Poisson distribution of sticky elements within the zone of influence:

$$P_N(n) = \frac{N^n e^{-N}}{n!}. \tag{6}$$

Here, P describes the probability of finding a particular number, n, of patches in the zone of influence, given that N is the average number of patches in the zone of influence. The parameter N is calculated based on the overall surface loading of patches. The average concentration of patches in the zone of influence $(N/\pi R_{zoi}^2)$ is equivalent to the average patch loading, ρ, i.e. on the x-axis of Fig. 2.

Particle capture requires that some number larger than a critical number of patches be present in the zone of influence. The Poisson distribution is therefore summed above this critical number to yield the complement of the cumulative distribution function, $P_A(N)$, which describes the probability of particle capture, as a function of the average number in the zone of influence.

$$P_A(N) = \sum_{n=critn\ \ num}^{\infty} P_N(n) \tag{7}$$

This expression is analogous to the simulated particle capture probability of Eq. (1). Shown in Fig. 7 is the probability for particle capture as a function of the average surface loading of patches on the x-axis, for 1 μm particles at different ionic strengths that vary the size of the zone of influence. The criterion for adhesion was based roughly on Fig. 6d, that more than 0.157 mg/m^2 of pDMAEMA, or 3000 cationic patches/μm^2 were present in the zone of influence. Fig. 7 is analogous to Fig. 2b: the probability of particle capture is analogous to the particle capture rate with the exception that the transport limit will obscure conditions where the capture probability approaches unity, placing an upper limit on what is seen experimentally, and with simulations.

Several important insights are gained from Fig. 7. First, the general shapes of the probability curves correspond semi-quantitatively to the observations for particle capture rate in Fig. 2b. The threshold shifts to the right with higher ionic strengths as a result of the random patch arrangement, combined with variations in the size of the zone of influence. This shift is shown in the inset of Fig. 7 for 3 particle sizes, analogous to Fig. 4. Also apparent in Fig. 7 is that the crossing of the data sets is a natural consequence of the Poisson distribution. When the zone of influence is small, smaller numbers of patches are involved in particle capture and the statistics of the smaller numbers give rise to the gradual slope in the rate/probability plots. As the size of the zone of influence increases, the statistics involve increasingly larger numbers of patches and the rate/probability plots become steeper, so that data sets cross.

The crossing point, ρ^*, in Fig. 7 is significant: as the zone of influence is increased, the shapes of the probability or rate plots

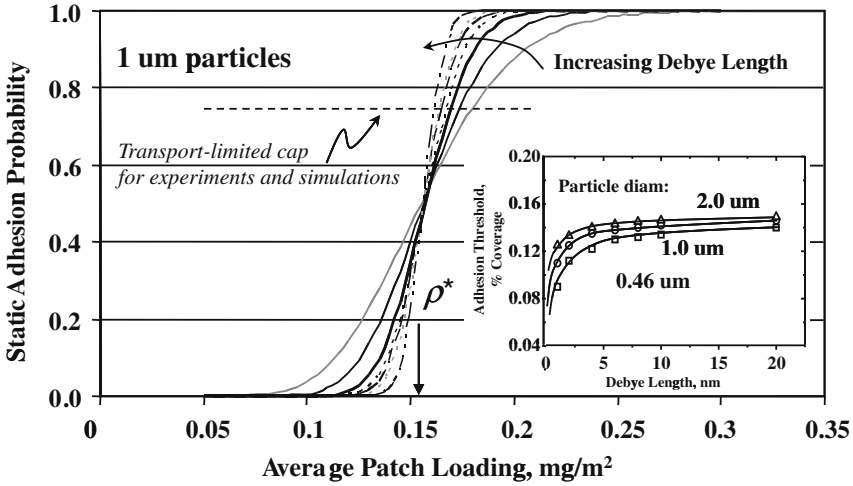

Fig. 7. Poisson calculations of the adhesion probability of 1 μm particles for different Debye lengths: 1, 2, 4, 8, 10, 20 nm. The inset shows how the threshold depends on particle size and Debye length, analogous to Fig. 4.

converge to a step function at this average patch concentration. The step function behavior corresponds to mean-field-like particle capture. Thus the crossing point of the rate plots reveal the mean-field like plateau, the limit of the adhesion threshold at large Debye lengths, in the state space in the inset of Fig. 7 or in Fig. 4. That this point corresponds to the average surface condition, in the purely statistical case of Fig. 7 is also clear: the crossing point, 0.157 mg/m^2, or 33% coverage, recovers the 3000 patches/μm^2 that was put into the statistical treatment as the local concentration needed for particle capture.

The crossing of the probability curves of Fig. 7 also reemphasizes that the ionic strength effects, which were mild in Fig. 3, are indeed real. In particular, the surprising finding in Fig. 3 that ionic strength stabilizes particles against adhesion/flocculation, is consistent with the statistical result, in Fig. 7. Indeed, all surface compositions above the crossing point in Fig. 7 (or Fig. 2) will become less adhesive with increases in ionic strength. These compositions comprise a small subset of the entire variable space, as indicated in Fig. 7, because the trend is truncated by transport-limited particle capture. The more classical increase of adhesion (and destabilization of suspensions) with increasing ionic strength occurs for surface compositions below the crossing point. This regime compares well with one case previously published case for particle adhesion on heterogeneous surfaces [49].

Also by way of comparison to prior literature, we find a Poisson treatment of the numbers of adsorbed PEI polycations needed to capture half-micron-scale latex [58,59]. Here comparison of the Poisson model to experiment revealed that between 2 and 3 adsorbed polymers are needed to capture each particle, consistent with our findings given the higher molecular weight of the PEI and lower pH, corresponding to lower background repulsion from the bare substrate. However, in this other work, the Poisson treatment was employed only to determine the critical number of coils needed for particle capture. Interpreting this critical number of adsorbed polymer molecules in the context of an equivalent contact area or R_{ZOI} (ie. depending ionic strength and particle size) was not considered. As a result no crossing of the experimental data or in the model was observed.

Despite its simplicity, the statistical model qualitatively captures the key features of the data in Figs. 2–4, and in the literature [58,59]. We were therefore motivated to extend this statistical treatment to a scaling treatment, developed in the appendix. We find that the random distribution of "stickers" when treated as Gaussian for large numbers of stickers (say above 10 or so) in the zone of influence, leads to a $(\kappa^{-1}a)^{-1/2}$ scaling of the adhesion threshold. This scaling is shown in Fig. 8a for the thresholds in the inset of Fig. 7, which were extrapolated from the curves in the main body of Fig. 7. The scaling is tested in Fig. 8b for the experimental data and simulations. The purely statistical model adheres well to this scaling for the range of parameters tested, while the experiments and simulations follow the scaling quite well, though not nearly as perfectly due primarily to hydrodynamic effects (and the history of particle motion over the surface).

While the analytical and scaling treatments reveal the importance of the statistical nature of the adhesive elements in the ability of the collector to capture particles, the entire development was based on the premise of a constant local concentration of adhesive elements in the zone of influence. This premise was shown to hold to the first order; however, real quantitative differences between Fig. 7 and the experimental and simulated data in Figs. 2 and 4 indicate that other factors are also important.

There remains a slight impact of particle size, beyond that anticipated by the statistical models. While hydrodynamic forces are small, they are sufficient to shift the threshold, as previously documented [89]. The fact that the particles are flowing over the surface also influences their probability of capture. Flow imparts a history-dependence along each particle's trajectory, so that the upstream pattern of patches on the surfaces influences whether the particle will be sufficiently close to the surface to adhere when a hot spot is encountered. If the particle is far from the surface but over a hot spot, it will approach the surface but be beyond the hot-spot when it gets close enough to be trapped, and may be repelled back again off the interface. Therefore, while the statistical treatments do an excellent job of explaining the general features of the heterogeneous interactions, the simulations more precisely match experiments because they take other important factors into account (and, indeed, reveal the critical patch density in the zone of influence required for adhesion, which was used as input for the statistical model.)

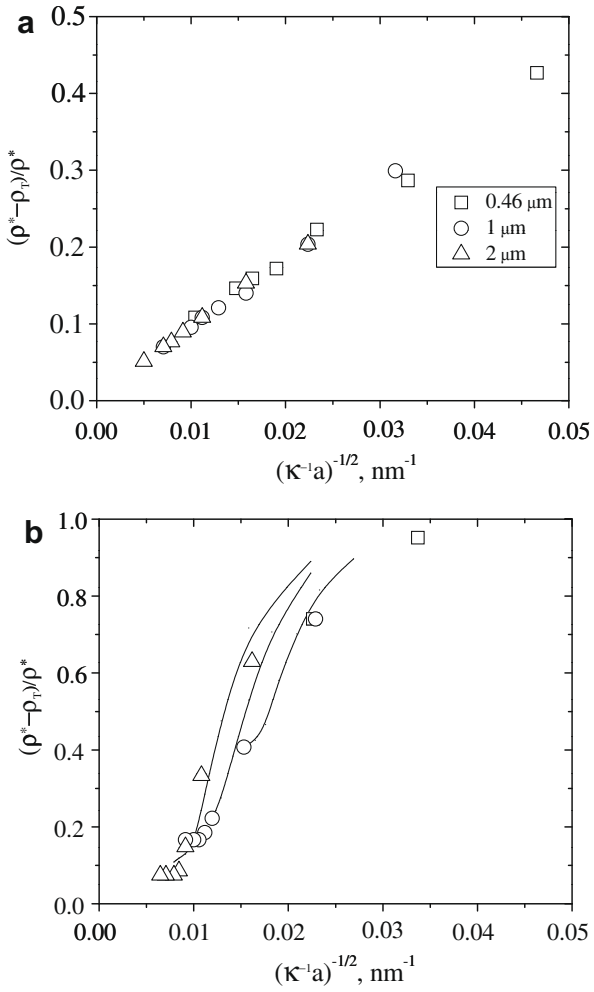

Fig. 8. (a) Test of scaling theory for the impact of ionic strength and particle size on the adhesion threshold, for the analytical model. The threshold values for the 1 μm particle were extrapolated directly from the curves in Fig. 7. A similar treatment was employed to obtain threshold values for 1 μm and 460 nm particles. (b) Test of scaling form for the experimental (symbols) and simulations (curves) from Fig. 4.

6. Summary

This work exploited an electrostatic system of tiny randomly-placed attractive surface elements to probe how heterogeneity alters the fundamental nature of colloidal interactions. While surface heterogeneity has been implicated in a number of counterintuitive interfacial behaviors, this work provided a clear picture of the influence of heterogeneities because the model system allowed for systematic variation in their density, with all interfaces being

well-characterized. The surface density of these random attractive elements was varied, along with the size of microparticles and the Debye length, and the full state space for particle capture from gentle flow was mapped. Simulations quantitatively matched the experimental results, confirming that the appropriate variables had been taken into consideration.

This study provided a detailed account of the general observation/speculation from the literature that attractive heterogeneities can be responsible for flocculation or particle adhesion when mean-field treatments predict stability. Because the heterogeneities were systematically varied in this investigation and no adjustable parameters were involved in the simulations or modeling, an explanation of particle capture (flocculation) was developed, based on the probability of finding adhesive surface regions. The simulations were central to the development of these arguments because they allowed access to features that were not measurable in experiments, such as the numbers of adhesive elements actually involved in particle capture. Indeed, a surprising result emerged, that the local surface concentration of adhesive elements beneath adhering particles was nearly constant. The simulations also facilitated an analogy between surface heterogeneities and receptors on cell surfaces: the numbers of adhesive elements were within the acceptable range of biological adhesion molecules.

Mean-field treatments like DLVO, with interactions governed by average electrostatic and van der Waals forces, have led us to the general concept that addition of salt produces particle adhesion and flocculation. Here we reported that with heterogeneous surfaces, salt can either help or hinder flocculation. In the limit where attractive heterogeneities are sparse, added salt screens the stabilizing repulsion, much like that on uniform surfaces (DLVO), destabilizing dispersions. At the opposite extreme, however, when attractive heterogeneities are dense, added salt also screens the attractive surface regions, producing a net stabilizing effect.

A final and overarching important concept developed in this work is the continuity of behaviors that can be observed with heterogeneous systems, as the heterogeneity lengthscale is varied relative to the size of the interactive area between surfaces. With large interactive areas, (for instance at low salt concentrations or for large particles), mean-field behavior is closely approximated while for small particles or conditions that produce small interactive areas (such as high salt concentrations) the system is governed by the distribution of fluctuations. This is the case for the full range of conditions, even though the surface topography always remains discretized, that is the adhesive elements are always isolated relative to the lengthscales of interest. This work demonstrated that the scaling law describing the threshold adhesion/flocculation condition scales as $(\kappa^{-1}a)^{1/2}$ when the adhesive heterogeneities are randomly distributed. This result derives only from a statistical treatment and neglects the effects of hydrodynamics, particle trajectory, and physico-chemical detail.

Acknowledgments

This work was supported by Grants NSF CBET-04-28455 and NSF BMS-08-05061. MMS thanks Greg Grayson for guidance on development of the scaling theory.

Appendix A. A scaling argument for the shape of the state space plot

The dependence of the adhesion threshold on particle radius, a, and Debye Length, κ^{-1}, in Fig. 4 and the inset of Fig. 7, can be understood by considering the statistics that govern the patches within the area of influence $A = \pi R_{zoi}^2$, where $R_{zoi} = 2\ (\kappa^{-1}a)^{1/2}$ as before. For adhesive elements randomly distributed on a surface, the Poisson distribution that describes their arrangement approaches a Gaussian form when approximately 10 or more patches are of interest. This condition is met in our case, as evidenced by the minimum numbers of patches needed for particle capture, in Fig. 6, which are most often greater than 20.

As one varies the average surface loading of patches (ρ, on the x-axes in the rate plots of Fig. 2), the distribution of the local patch concentration shifts, as shown in Fig. A.1. Here the local number of patches, n on the x-axis, that one might find within the area of influence, A, exhibits a bell-shape, with the distributions shifting to the right as the surface is loaded with greater average densities of patches, ρ_1, ρ_2, etc. N_1 and N_2 correspond to the mean of the distribution in Fig. A.1 for average surface loadings ρ_1, ρ_2, etc. The distribution also widens as this average loading is increased.

The experiments and simulations have shown that particle capture can occur only when the particle encounters a critical number of patches n^*, which, roughly, is a fixed number for our experimental conditions and for a particular area of the zone of influence A, in Fig. 6c. The adhesion thresholds seen in Figs. 2 and 4, are exceeded only when the average concentration of patches gives rise to a finite likelihood of a particle finding n^* patches the zone of influence. Fig. A.1 shows that this can be expected only when the tail of the distribution crosses n^* substantially.

We could write this latter criterion by saying that the average patch number inside the zone of influence at the threshold, N_T must be within a standard deviation $\langle \Delta n^2 \rangle^{1/2}$ of the target, n^*:

$$N_T + \langle \Delta n^2 \rangle^{1/2} = n^* \tag{A.1}$$

For Gaussian statistics, the standard deviation is related to the average, $\langle \Delta n^2 \rangle^{1/2} = N^{1/2}$, which gives

$$N_T + N^{1/2} = n^*. \tag{A.2}$$

For N and $n^* \gg 1$ this requirement becomes

$$n^* - N_T \approx n^{*1/2}. \tag{A.3}$$

While we observed that the concentration of patches inside the zone of influence was fixed at some particular surface concentration ρ^* (of Fig. 6d), n^* (of Fig. 6c) is area-dependent:

$$n^* = \pi R_{zoi}^2 \rho^* \tag{A.4}$$

Likewise, the average of the distribution, N is related to ρ, the average loading, for instance on the x-axis of Figs. 2 and 4:

$$N = \pi R_{zoi}^2 \rho \tag{A.5a}$$

so that at the threshold

$$N_T = \pi R_{zoi}^2 \rho_T \tag{A.5b}$$

Therefore, Eq. (A.3) becomes

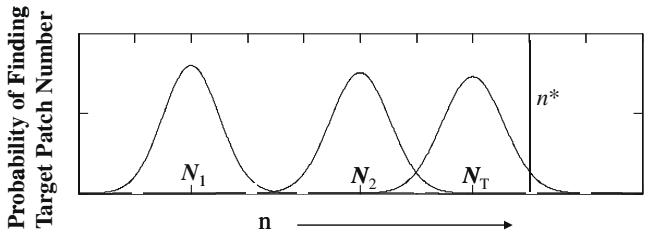

Fig. A.1. The probability of finding a target number, n, of patches in the zone of influence, when N_1, N_2, etc. are the average numbers of patches in the zone of influence. n^* is the critical number of patches in the zone of influence needed for particle capture, such as on the y-axis of Fig. 6c. N_T is the average number of patches in the zone of influence at the adhesion threshold, related to the overall patch loading at the adhesion threshold in Fig. 2.

$$\pi R_{zoi}^2 \rho^* - \pi R_{zoi}^2 \rho_T \approx (\pi R_{zoi}^2 \rho^*)^{1/2}, \tag{A.6}$$

or

$$\rho^* - \rho_T \approx (\pi R_{zoi}^2 \rho^*)^{1/2} = (1/2)(\rho^*/\pi)^{1/2}(\kappa^{-1}a)^{-1/2}. \tag{A.7}$$

The crossing of the rate plot data near a capture probability of 50% in Fig. 7 provide an indication of the critical concentration of patches in the zone of influence, ρ^*. The parameter ρ^* is a system-specific constant that also appears as the concentration of patches in the zone of influence needed for particle capture. Therefore both ρ^* and ρ_T are known, with the former being a constant, and the latter dependent on particle size and ionic strength in the manner observed in the state space of Fig. 2.

Eq. (A.7) therefore predicts an inverse square root scaling with Debye length and particle size for the adhesion threshold about its plateau value in state space.

References

[1] E. Martines, L. Csaderova, H. Morgan, A.S.G. Curtis, M.O. Riehle, Colloids Surf. A Physicochem. Eng. Aspects 318 (2008) 45–52.
[2] S. Bhattacharjee, C.H. Ko, M. Elimelech, Langmuir 14 (1998) 3365–3375.
[3] K. Shellenberger, B.E. Logan, Environ. Sci. Technol. 36 (2002) 184–189.
[4] J.B. Kortright, S.K. Kim, G.P. Denbeaux, G. Zeltzer, K. Takano, E.E. Fullerton, Phys. Rev. B 64 (2001).
[5] J. Mahnke, J. Stearnes, R.A. Hayes, D. Fornasiero, J. Ralston, Phys. Chem. Chem. Phys. 1 (1999) 2793–2798.
[6] E. Tombacz, M. Szekeres, Appl. Clay Sci. 34 (2006) 105–124.
[7] V.M. Gun'ko, R. Leboda, V.V. Turov, F. Villieras, J. Skubiszewska-Xieba, S. Chodorowski, M. Marciniak, J. Colloid Interface Sci. 238 (2001) 340–356.
[8] G.V. Lubarsky, M.R. Davidson, R.H. Bradley, Surf. Sci. 558 (2004) 135–144.
[9] J. Song, J.F.L. Duval, M.A.C. Stuart, H. Hillborg, U. Gunst, H.F. Arlinghaus, G.J. Vancso, Langmuir 23 (2007) 5430–5438.
[10] J.A. Brant, K.M. Johnson, A.E. Childress, Colloids Surf. A Physicochem. Eng. Aspects 280 (2006) 45–57.
[11] A. Mendez-Vilas, J. Diaz, M.G. Donoso, A.M. Gallardo-Moreno, M.L. Gonzalez-Martin, Antonie Van Leeuwenhoek Int. J. Gen. Mol. Microbiol. 89 (2006) 495–509.
[12] L.S. Dorobantu, S. Bhattacharjee, J.M. Foght, M.R. Gray, Langmuir 24 (2008) 4944–4951.
[13] Y.F. Dufrene, Curr. Opin. Microbiol. 6 (2003) 317–323.
[14] T.A. Camesano, N.I. Abu-Lail, Biomacromolecules 3 (2002) 661–667.
[15] I.N. Plaksin, R.S. Shafeev, Dokl. Akademii Nauk Sssr 121 (1958) 145–148.
[16] F. Bartoli, G. Burtin, J. Guerif, Geoderma 54 (1992) 259–274.
[17] Z. Wang, S.L. Hemmer, D.M. Friedrich, A.G. Joly, J. Phys. Chem. A 105 (2001) 6020–6023.
[18] C. Priest, N. Stevens, R. Sedev, W. Skinner, J. Ralston, J. Colloid Interface Sci. 320 (2008) 563–568.
[19] M. Strobel, V. Jones, C.S. Lyons, M. Ulsh, M.J. Kushner, R. Dorai, M.C. Branch, Plasmas Polym. 8 (2003) 61–95.
[20] C.P. Fang, J. Drelich, Langmuir 20 (2004) 6679–6684.
[21] A. Sharma, R. Konnur, K. Kargupta, Physica A Stat. Mech. Appl. 318 (2003) 262–278.
[22] I.S. Chang, P. Le Clech, B. Jefferson, S. Judd, J. Environ. Eng. ASCE 128 (2002) 1018–1029.
[23] Y. Bessiere, D.F. Fletcher, P. Bacchin, J. Membrane Sci. 313 (2008) 52–59.
[24] B.S. Gupta, I. Reiniati, M.P.G. Laborie, Colloids Surf. A Physicochem. Eng. Aspects 302 (2007) 388–395.
[25] A. Aymonier, E. Papon, G. Castelein, A. Brogly, P. Tordjeman, J. Colloid Interface Sci. 268 (2003) 341–347.
[26] Y.W. Huang, V.K. Gupta, J. Chem. Phys. 121 (2004) 2264–2271.
[27] R. Miller, Z. Guo, E.A. Vogler, C.A. Siedlecki, Biomaterials 27 (2006) 208–215.
[28] P.Y. Meadows, G.C. Walker, Langmuir 21 (2005) 4096–4107.
[29] R. Bos, H.C. van der Mei, J. Gold, H.J. Busscher, FEMS Microbiol. Lett. 189 (2000) 311–315.
[30] R. Bos, H.C. vanderMei, J. deVries, H.J. Busscher, Colloids Surf. B Biointerfaces 7 (1996) 101–112.
[31] A.N. Mundhekar, D.C. Bullard, D.F. Kucik, Am. J. Physiol. Cell Physiol. 291 (2006) C130–C137.
[32] M.B. Kim, I.H. Sarelius, Am. J. Physiol. Heart Circ. Physiol. 287 (2004) H2705–H2711.
[33] S.L. Walker, J.E. Hill, J.A. Redman, M. Elimelech, Appl. Environ. Microbiol. 71 (2005) 3093–3099.
[34] S.E. Truesdail, J. Lukasik, S.R. Farrah, D.O. Shah, R.B. Dickinson, J. Colloid Interface Sci. 203 (1998) 369–378.
[35] S.L. Walker, J.A. Redman, M. Elimelech, Langmuir 20 (2004) 7736–7746.
[36] F. Martinez-Pedrero, M. Tirado-Miranda, A. Schmitt, F. Vereda, J. Callejas-Fernandez, Colloids Surf. A Physicochem. Eng. Aspects 306 (2007) 158–165.
[37] J.F. Jones, G.L. Holtzer, C. Snyder, A.M. Yake, D. Velegol, Colloids Surf. A Physicochem. Eng. Aspects 267 (2005) 79–85.
[38] P. Taboada-Serrano, V. Vithayaveroj, S. Yiacoumi, C. Tsouris, Environ. Sci. Technol. 39 (2005) 6352–6360.
[39] A.H. Cardoso, C.A.P. Leite, F. Galembeck, Colloids Surf. A Physicochem. Eng. Aspects 181 (2001) 49–55.
[40] Y.K. Leong, Colloid Polym. Sci. 277 (1999) 299–305.
[41] N. Bohm, W.M. Kulicke, Colloid Polym. Sci. 275 (1997) 73–81.
[42] G. Durandpiana, F. Lafuma, R. Audebert, J. Colloid Interface Sci. 119 (1987) 474–480.
[43] F. Mabire, R. Audebert, C. Quivoron, J. Colloid Interface Sci. 97 (1984) 120–136.
[44] J. Gregory, J. Colloid Interface Sci. 42 (1973) 448–456.
[45] J. Gregory, J. Colloid Interface Sci. 55 (1976) 35–44.
[46] E. Kokkoli, C.F. Zukoski, Langmuir 17 (2001) 369–376.
[47] M. Elimelech, J.Y. Chen, Z.A. Kuznar, Langmuir 19 (2003) 6594–6597.
[48] J.E. Tobiason, Colloids Surf. 39 (1989) 53–77.
[49] L.F. Song, P.R. Johnson, M. Elimelech, Environ. Sci. Technol. 28 (1994) 1164–1171.
[50] J. Gregory, A.J. Wishart, Colloids Surf. 1 (1980) 313–334.
[51] M. Elimelech, C.R. Omelia, Langmuir 6 (1990) 1153–1163.
[52] M. Elimelech, Water Res. 26 (1992) 1–8.
[53] J. Zhang, S. Srivastava, R. Duffadar, J.M. Davis, V.M. Rotello, M.M. Santore, Langmuir 24 (2008) 6404–6408.
[54] N. Nazemifard, J.H. Masliyah, S. Bhattacharjee, J. Colloid Interface Sci. 293 (2006) 1–15.
[55] Z. Adamczyk, B. Siwek, E. Musial, Colloids Surf. A Physicochem. Eng. Aspects 214 (2003) 219–229.
[56] Z. Adamczyk, B. Siwek, K. Jaszczolt, P. Weronski, Colloids Surf. A Physicochem. Eng. Aspects 249 (2004) 95–98.
[57] Z. Adamczyk, K. Jaszczolt, B. Siwek, Appl. Surf. Sci. 252 (2005) 723–729.
[58] Z. Adamczyk, A. Michna, M. Szaraniec, A. Bratek, J. Barbasz, J. Colloid Interface Sci. 313 (2007) 86–96.
[59] Z. Adamczyk, A. Zembala, A. Michna, J. Colloid Interface Sci. 303 (2006) 353–364.
[60] W.P. Johnson, M.P. Tong, Environ. Sci. Technol. 40 (2006) 5015–5021.
[61] J.Y. Chen, J.F. Klemic, M. Elimelech, Nano Lett. 2 (2002) 393–396.
[62] N.A.M. Araujo, A. Cadilhe, V. Privman, Phys. Rev. E 77 (2008).
[63] X.Z. Jin, N.H.L. Wang, G. Tarjus, J. Talbot, J. Phys. Chem. 97 (1993) 4256–4258.
[64] M.M. Santore, J. Zhang, S. Srivastava, V.M. Rotello, Langmuir 25(1) 84–96.
[65] N. Hansupalak, Ph.D. Thesis, Lehigh University, 2003.
[66] N. Kozlova, M.M. Santore, Langmuir 22 (2006) 1135–1142.
[67] M.M. Santore, N. Kozlova, Langmuir 23 (2007) 4782–4791.
[68] Y. Shin, J.E. Roberts, M.M. Santore, Macromolecules 35 (2002) 4090–4095.
[69] Y.W. Shin, J.E. Roberts, M.M. Santore, J. Colloid Interface Sci. 247 (2002) 220–230.
[70] N. Hansupalak, M.M. Santore, Macromolecules 37 (2004) 1621–1629.
[71] N. Hansupalak, M.M. Santore, Langmuir 19 (2003) 7423–7426.
[72] R.D. Duffadar, J.M. Davis, J. Colloid Interface Sci. 308 (2007) 20–29.
[73] Y.W. Shin, J.E. Roberts, M. Santore, J. Colloid Interface Sci. 244 (2001) 190–199.
[74] Z.G. Fu, M.M. Santore, Colloids Surf. A Physicochem. Eng. Aspects 135 (1998) 63–75.
[75] A. Vanblaaderen, A. Vrij, Langmuir 8 (1992) 2921–2931.
[76] W. Stober, A. Fink, E. Bohn, J. Colloid Interface Sci. 26 (1968) 62.
[77] M.M. Santore, Curr. Opin. Colloid Interface Sci. 10 (2005) 176–183.
[78] R.D. Duffadar, J.M. Davis, J. Colloid Interface Sci. 326 (2008) 18–27.
[79] M.A. Leveque, Ann. Mines 13 (1928) 284.
[80] R. Duffadar, Ph.D. Thesis, 2008.
[81] N.A. Mody, M.R. King, Langmuir 23 (2007) 6321–6328.
[82] A.J. Banchio, J.F. Brady, J. Chem. Phys. 118 (2003) 10323–10332.
[83] A. Li, G. Ahmadi, Aerosol Sci. Technol. 16 (1992) 209–226.
[84] M.P. Tong, T.A. Camesano, W.P. Johnson, Environ. Sci. Technol. 39 (2005) 3679–3687.
[85] L.F. Song, M. Elimelech, J. Colloid Interface Sci. 167 (1994) 301–313.
[86] A.J. Goldman, R.G. Cox, H. Brenner, Chem. Eng. Sci. 22 (1967) 653.
[87] M.R. King, D.A. Hammer, Biophys. J. 81 (2001) 799–813.
[88] M.R. King, S.D. Rodgers, D.A. Hammer, Langmuir 17 (2001) 4139–4143.
[89] S. Kalasin, M.M. Santore, Langmuir 24 (2008) 4435–4438.